A Two-Dimensional Doppler-Radiometer for Earth Observation

Adriano J. Camps, *Member, IEEE,* and Calvin T. Swift, *Fellow, IEEE*

***Abstract*—Compared to synthetic aperture radars (SARs), the angular resolution of microwave radiometers is quite poor. Traditionally, it has been limited by the physical size of the antenna. However, the angular resolution can be improved by means of aperture synthesis interferometric techniques. A narrow beam is synthesized during the image formation processing of the cross-correlations measured at zero-lag between pairs of signals collected by an array of antennas. The angular resolution is then determined by the maximum antenna spacing normalized to the wavelength (baseline). The next step in improving the angular resolution is the Doppler-Radiometer, somehow related to the super-synthesis radiometers and the Radiometer-SAR. This paper presents the concept of a three-antenna Doppler-Radiometer for 2-D imaging. The performance of this instrument is evaluated in terms of angular/spatial resolution and radiometric sensitivity ,and an L-band illustrative example is presented.**

***Index Terms*—Interferometry, radiometry, sparse arrays.**

I. Introduction

THE CONCEPT of a synthetic-aperture radiometer using matched filtering techniques goes back to the early 1970s with the work of Mel'nik [1], [2]. More recently, Komiyama [3]–[7] and Edelsohn [8], [9] have presented some theoretical results and measurements in different configurations on both artificial and natural targets. Unfortunately, few details are given in these references, particularly with regard to specifying radiometric sensitivity. This paper presents a detailed analysis of the impulse response, the spatial resolution and the radiometric sensitivity of a two-dimensional (2-D) Doppler-radiometer,[1] including spatial decorrelation effects due to the finite bandwidth, not included in former analyses.

The configuration under study is shown in Fig. 1. In order to simplify the algebraic equations without loss of generality, results will be derived for a plane Earth. Three antennas are mounted on a platform at a height $z = H_0$, that moves along the X-axis at constant speed v.

Manuscript received December 15, 1999; revised July 23, 2000. This work was supported in part by Fellowship PR98 0 046 131 105 of the Spanish Ministry of Education and Culture.

A. J. Camps is with the Department of Signal Theory and Communications, Universitat Politècnica de Catalunya, 08034 Barcelona, Spain.

C. T. Swift is with the Microwave Remote Sensing Laboratory, University of Massachusetts, Amherst, MA 01003 USA.

Publisher Item Identifier S 0196-2892(01)05469-9.

[1]The name Doppler-radiometer comes from the phase variation of the cross-correlations that would be measured from the signals collected by the antennas due to the variation of the differential propagation delay. For the pixels being focused, the time-dependent differential delay is compensated for by a matched filter. The name Doppler-radiometer does not mean that there is a significant Doppler shift in the frequency of the signals collected by the antennas.

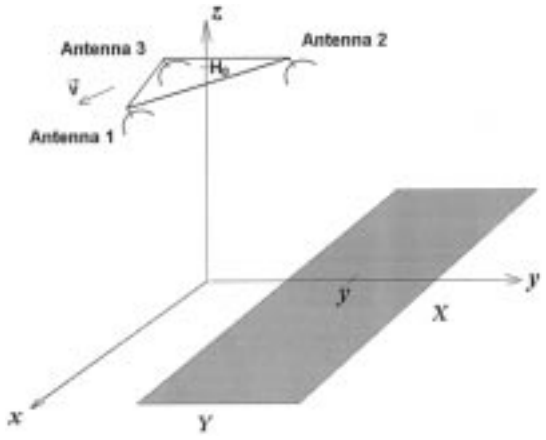

Fig. 1. Scan geometry of a Doppler-radiometer.

The positions of these antennas are given by

$$\begin{aligned} R_1(t) &= (+D_1/2 + vt,\, 0,\, H_0), \\ R_2(t) &= (-D_1/2 + vt,\, +D_2,\, H_0), \\ R_3(t) &= (-D_1/2 + vt,\, -D_2,\, H_0). \end{aligned} \tag{1}$$

Antenna 1 is shared between the baselines 12 and 13 formed by antenna pairs 1–2 and 1–3

$$\begin{aligned} (u_{12},\, v_{12}) &= (R_2(t) - R_1(t))/\lambda \\ &= (-D_1,\, +D_2)/\lambda \mathrel{\hat{=}} (u,\, v), \\ (u_{13},\, v_{13}) &= (R_3(t) - R_1(t))/\lambda \\ &= (-D_1,\, -D_2)/\lambda \mathrel{\hat{=}} (u,\, -v) \end{aligned} \tag{2}$$

where $\lambda = c/f_0$ is the electromagnetic wavelength at the center frequency.

The antennas are assumed to have all the same antenna voltage pattern $F_n(x, y) = \exp(-(y - \overline{y})^2/(2Y^2))\exp(-x^2/(2X^2))$, and the receivers all the same frequency response, modeled by a Gaussian filter $H(f) = \exp(-\pi(f - f_0)^2/(2B^2))$ centered at $f = f_0$, with equivalent noise bandwidth B, so that the fringe-washing function can be modeled by $\tilde{r}(t) = \exp(-\pi B^2 t^2)$ [10].

The cross-correlation of the signals $b_k(t)$ and $b_l(t)$ collected by antennas k and l is given by

$$\overline{V}_{kl} = \tfrac{1}{2}\langle b_k(t - \tau_k(t)) b_l^*(t - \tau_l(t))\rangle \tag{3}$$

where $\tau_k(t)$ and $\tau_l(t)$ are instrumental delays introduced to compensate for different transit times from a given pixel in the field of view to the antennas k and l (Fig. 2).

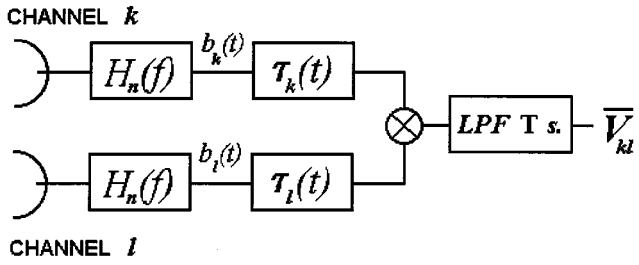

Fig. 2. Diagram of a baseline of a Doppler-radiometer.

II. Doppler-Radiometer with Adjustable Delay Compensation

The configuration under study is similar to the one described by Mel'nik [1], who described a baseline and a matched filter to track the differential delay from a focused pixel (x_0, y_0) in the field of view and the two antennas [$\tau_k(t) = \tau_k(x_0, y_0, t)$ and $\tau_l(t) = \tau_l(x_0, y_0, t)$]. In this sense, the Doppler-radiometer concept is somewhat similar to the VLBI interferometry in which adjustable delays in the channels are used to "stop the fringes" [11], [12]. However, in VLBI observations, the objects under observation are in the far field of the array. The rotation due to the Earth is used to synthesize different baselines, corresponding to different spatial frequencies of the Fourier transform of the brightness temperature of the sky, which is then recovered by deconvolution techniques [12], [13]. In the Doppler-radiometer, the moving baseline observes the object during T seconds. Since the product vT may be comparable to the platform height, the objects are in the near field of the synthetic aperture. The image is formed pixel by pixel by matched filtering the signals collected by the antennas so as to compensate for the propagation delay (different in each observation). The outputs are then cross-correlated.

Fig. 2 shows the hardware configuration. The adjustable delays $\tau_1(t) = \hat{r}_1(t)/c$ and $\tau_2(t) = \hat{r}_2(t)/c$ partially compensate the propagation delays $r_1(t)/c$ and $r_2(t)/c$ from the pixel being focused (x_0, y_0) to the antennas (A1.2)–(A1.5). At a given instant t, the delay error $\Delta\tau(t) = [r_1(t) - \hat{r}_1(t) - r_2(t) + \hat{r}_2(t)]/c$ of nonfocused pixels (x_1, y_1) produces the two following effects in the output.

- Due to decorrelation effects, the amplitude decreases as the fringe-washing function $\tilde{r}(\Delta\tau(t)) = \exp(-\pi B^2 \Delta\tau^2(t))$.
- Also, except for the focused pixel $(\Delta\tau(t) = 0)$, the phase varies as[2] $\exp(j\omega_0 \Delta\tau(t))$.

The output of the low-pass filter then filters out all the AC components (contributions from nonfocused pixels) and retains the DC component (from the focused one). The response of the baseline 1–2 is given by (A1.13), as in (4), shown at the bottom of the page, where

k	Boltzmann's constant;
B	receiver's noise bandwidth as defined in Section I;
$W = B/f_0$	relative bandwidth;
Ω_{pix} and Ω_{ant}	solid angles subtended by the pixel being imaged and the antenna;
T_{B0}	brightness temperature at (x_0, y_0);

and $\Delta x = x_1 - x_0$, $\Delta y = y_1 - y_0$, and $R_0 = \sqrt{H_0^2 + y_0^2}$. From (A1.13) to (4), the integration time T has been set to[3] $T = \sqrt{\pi} X/v$.

Since $(u_{13}, v_{13}) = (u_{12}, -v_{12}) \hat{=} (u, -v)$, the response of the baseline 1–3 is obtained from (4), substituting v by $-v$. The interested reader is referred to the Appendix for the mathematical details leading to (4).

A. Doppler-Radiometer Spatial Resolution

In the coherent case $(W = 0)$, near the focused pixel ($x_1 \approx x_0$ and $y_1 \approx y_0$) (4) represents a Gaussian function whose maximum is located along the line $\Delta y = v/u \Delta x$ and passes through the focused point (x_0, y_0). In a similar way, the response of the baseline 1–3 is a Gaussian function whose maximum is located along the line $\Delta y = -v/u \Delta x$ that passes through the focused point (x_0, y_0). Consequently, baselines 1–2 and 1–3 achieve spatial resolution along the directions $\Delta y = -u/v \Delta x$ and $\Delta y = u/v \Delta x$, respectively. 2-D spatial resolution is achieved computing the geometric mean of both outputs. If, for mathematical simplicity we assume that

$$\frac{2}{\pi} W \frac{\Delta\rho}{\varepsilon_\rho} \ll 1 \quad \text{and} \quad \sqrt{2} \frac{\Delta x X}{R_0^{3/2} \lambda^{1/2}} \ll 1$$

[2]For simplicity, without loss of generality, it has been assumed that the adjustable delays are inserted at f_0. See [13] for an analysis of the response of a VLBI baseline when delays are inserted at intermediate frequency. If $H(f)$ is not symmetrical with respect to f_0, the local oscillator is not at f_0, or the channels frequency response is not the same an additional phase term $\exp(j\phi(f))$ appears [10].

[3]The antenna radiation pattern at $x = \pm vT/2$ is $\exp(-\pi/4) = 0.46$, which corresponds approximately to the points at half power.

$$\overline{V}_{12} = kB \frac{\Omega_{pix}}{\Omega_{ant}} T_{B0} \exp\left(-\frac{(y_0 - \overline{y})^2}{Y^2}\right) \frac{\sqrt{\pi} X}{vT} \frac{\exp\left(-\dfrac{\pi^2 (y_0/R_0^3)^2 (\Delta x v - \Delta y u)^2}{\dfrac{1}{X^2}\left[1 + \left(\dfrac{\Delta x^2 X^2}{R_0^3 \lambda}\right)^2 + \pi W^2 \left(\dfrac{y_0 X}{R_0^3}\right)^2 (\Delta x v - \Delta y u)^2\right]}\right)}{\sqrt{1 + \left(\dfrac{\Delta x^2 X^2}{R_0^3 \lambda}\right)^2 + \pi W^2 \left(\dfrac{y_0 X}{R_0^3}\right)^2 (\Delta x v - \Delta y u)^2}} \tag{4}$$

then

$$\sqrt{\overline{V}_{12}\overline{V}_{13}} \approx kB\,\frac{\Omega_{pix}}{\Omega_{ant}}\,T_{B0}\exp\left(-\frac{(y_0-\overline{y})^2}{Y^2}\right) \cdot \exp\left(-\left(\frac{\Delta\rho}{\varepsilon_\rho}\right)^2\right), \tag{5}$$

$$\varepsilon_\rho \hat{=} \frac{R_0^3}{\pi y_0 u X} \tag{6}$$

where ε_ρ is a measure of the spatial resolution at $1/e$, $\Delta x \hat{=} \Delta\rho\cos\phi$ and $\Delta y \hat{=} \Delta\rho\sin\phi$, and $u = v$ so as to achieve the same spatial resolution in both directions.[4] That is, near the focused pixel the impulse response is a 2-D Gaussian function. From now on, the constants k and B will be implicitly understood, and the output $\sqrt{\overline{V}_{12}\overline{V}_{13}}$ will have units of K.

The antenna half-power footprint in the along-track direction is given by

$$\Delta X_{-3\,\mathrm{dB}} = 2\sqrt{\ln 2}X = \frac{R_0}{l_x} \tag{7}$$

where l_x is the antenna size normalized to the wavelength in the x direction. Using eqns. (6) and (7), the spatial resolution at half-power is given by

$$\Delta\rho_{-3\,\mathrm{dB}} = 2\sqrt{\ln 2}\varepsilon_\rho = \frac{8\ln 2}{\pi}\,\frac{H_0}{\sin(2\theta)}\,\frac{l_x}{u}. \tag{8}$$

As in SAR systems, spatial resolution improves for smaller antennas (larger integration time) and longer baselines. Spatial resolution is optimum at $\theta = 45°$ for which $\Delta\rho_{-3\,\mathrm{dB}} \approx 1.77H_0l_x/u$ and degrades at swath edges. This is, the spatial resolution of a synthetic aperture radar is degraded by a factor of approximately H_0/D_1.

B. Doppler-Radiometer Radiometric Sensitivity

Assuming that all receivers have the same system temperature, the radiometric sensitivity of each baseline is given by [14], [15]

$$\sigma^2_{\overline{V}^2_{kl}} = \sigma^2_{V_{kl,\,r}} + \sigma^2_{Vkl,\,i} \approx \frac{T^2_{\mathrm{sys}}}{\sqrt{2}B\tau} \tag{9}$$

where $T_{\mathrm{sys}} = T_A + T_R$ is the system temperature. The $\sqrt{2}$ factor comes from the Gaussian model for the channel frequency response [15], and $\tau \equiv T = \sqrt{\pi}X/v$ is the integration time.[5] Equation (9) is valid for this type of radiometer since the frequency response of the matched filter (adjustable delay line) is flat and the frequency response of the cascade filter remains unchanged.

[4]If the matched-filter is applied after the cross-correlation as in the super-synthesis radiometer [3]–[7] and $W = 0$, it can be demonstrated that the same spatial resolution is achieved. However, in this case, it can be demonstrated that the integration time $\tau^{\mathrm{sup\text{-}synth}} \approx \varepsilon_\rho/v$ is much lower than for the Doppler-radiometer $\tau^{\mathrm{Doppler\text{-}rad}} \approx X/v$.

[5]For analog or multibit correlators, the effective integration time equals the integration time $\tau_{\mathrm{eff}} = \tau$. For other correlator types $\tau_{\mathrm{eff}} = \tau/Q$, for instance, $Q = 2.46$ or 1.82 for 1 bit/2 level digital correlators at sampling frequency $f_s = 2B$ or $f_s = 4B$ and $Q = 1.29$ or 1.14 for two bit by two-bit digital correlators at sampling frequency $f_s = 2B$ or $f_s = 4B$ [16].

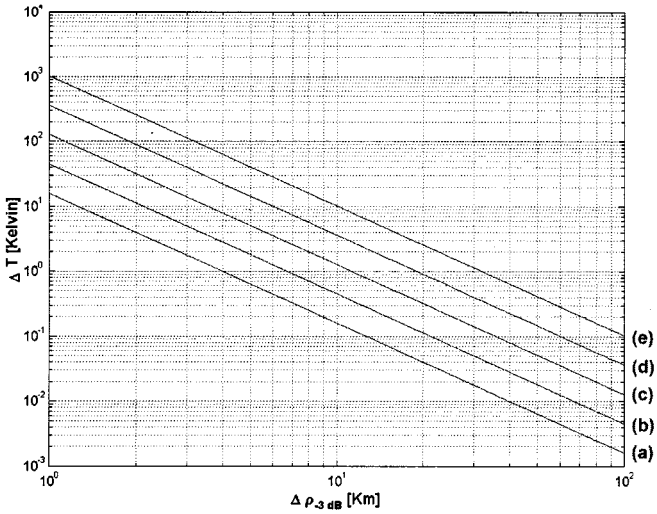

Fig. 3. Tradeoff of radiometric sensitivity versus spatial resolution for different swath widths: $\Delta X_{-3\,\mathrm{dB}} = \Delta Y_{-3\,\mathrm{dB}}$. (a) 50 km, (b) 100 km, (c) 200 km, (d) 400 km,and (e) 800 km. For a given $\Delta X_{-3\,\mathrm{dB}}$, the radiometric sensitivity can be improved by increasing the beam filling factor, e.g., reducing the swath width $\Delta Y_{-3\,\mathrm{dB}}$.

If $\overline{V}_{12}$ and $\overline{V}_{13}$ are the mean values of V_{12} and V_{13}, and ΔV_{12} and ΔV_{13} are the errors in the measurements, the variance of the geometric mean of V_{12} and V_{13} can be estimated from

$$\sqrt{\overline{V}_{12}(1+\Delta\overline{V}_{12}/\overline{V}_{12})\overline{V}_{13}(1+\Delta\overline{V}_{13}/\overline{V}_{13})} \approx \sqrt{\overline{V}_{12}\overline{V}_{13}}\left[1+\frac{1}{2}\,\frac{\Delta\overline{V}_{12}}{\overline{V}_{12}}+\frac{1}{2}\,\frac{\Delta\overline{V}_{13}}{\overline{V}_{13}}\right]. \tag{10}$$

Since at the center of the pixel $\overline{V}_{12} \approx \overline{V}_{13}$

$$\sigma_{\sqrt{\overline{V}_{12}\overline{V}_{13}}} \approx \frac{1}{2}\,\sigma_{V_{kl}} = \frac{1}{2}\,\frac{T_{\mathrm{sys}}}{\sqrt{\sqrt{2}BT}}. \tag{11}$$

However, the actual measurements are reduced by the beam-filling factor $\Omega_{pix}/\Omega_{ant} \approx \varepsilon^2_\rho/XY$ (5). The actual brightness temperature of each pixel is obtained after compensation for this factor $T_{B0} = \sqrt{\overline{V}_{12}\overline{V}_{13}}XY/\varepsilon^2_\rho$, and consequently, the radiometric sensitivity is degraded by the inverse of the beam-filling factor

$$\Delta T = \frac{1}{2}\,\frac{T_{\mathrm{sys}}}{\sqrt{\sqrt{2\pi}B/v}}\,\frac{\sqrt{XY}}{\varepsilon^2_\rho}. \tag{12}$$

Fig. 3 shows the tradeoff between spatial resolution and radiometric sensitivity for different swath widths. For a given spatial resolution, radiometric sensitivity improves for smaller swath widths (lower degree of array thinning). In the limiting case that $X = Y = \varepsilon^2_\rho$, the antennas overlap and the system tends to a real aperture radiometer.

C. Other Considerations in Doppler-Radiometers

At this point, six considerations regarding the practical implementation and limitations of this system have to be made.

- *Variation of the emissivity during integration.* For the sake of mathematical simplicity, in the former development, the emissivity has been assumed to be constant. However,

during the observation of a pixel, both the incidence angle θ_i and the azimuth angle φ_i vary[6]

$$\cos\theta_i = \frac{H_0}{\sqrt{R_0^2 + (vt)^2}},$$
$$tg\varphi_i = \frac{vt}{y_0} \qquad \text{for } |vt| \le \frac{\sqrt{\pi}}{2} X. \tag{13}$$

The worst case occurs for the pixels closest to the ground-track $y_0 = \overline{y} - \overline{Y}_{-3\,\mathrm{dB}}/2$.

- *Variation of the solid angle of the pixel during integration.* In addition, the solid angle subtended by a pixel was supposed to be constant, while it varies with the range and the incidence angle

$$\Omega_{pix} = \frac{\varepsilon_\rho^2}{R_0^2 + (vt)^2}\cos\theta_i, \qquad \text{for } |vt| \le \frac{\sqrt{\pi}}{2} X. \tag{14}$$

As previously, the worst case occurs for the pixels closest to the ground-track.

- *Delay tracking.* The time resolution required for a 1% precision in amplitude measurements is $\Delta t = 1/16B$ [13]. At L-band, the allocated band for passive observations is 1400 MHz to 1427 MHz. If only 20 MHz are used, then the required sampling period is $\Delta t \approx 3$ ns ($f_s = 320$ MHz).
- *Frequency stability.* The relative frequency stability between the local oscillators must be $\partial f/f_0 \le 1/(2\pi f_0 \tau)$ [13]. At L-band $\partial f/f_0 \le 2 \cdot 10^{-12}$, for $\tau = 60$ s.
- *Different channel frequency responses.* Channel frequency responses must be very similar [11, pp. 195–201]. However, frequency mismatches can be characterized [10] and included in the matched filtering process.
- *Computational load.* In order to form the image of a pixel, the output voltages of the receivers must be sampled every Δt seconds during an integration time T. Therefore, the total number of samples per receiver is

$$N = \frac{T}{\Delta t} = 16\sqrt{\pi}\,\frac{XB}{v}. \tag{15}$$

Once the sequences are aligned to compensate for the differential delay, $2N$ products and $2N$ summations are required to obtain V_{12} and V_{13}. The magnitudes involved represent a huge amount of products to focus every single pixel. However, if the signals are sampled with two levels (1 bit), products could be implemented with exclusive-OR gates, and the summations with counters and shift registers.[7] The number of complex-correlators is equal to the inverse of the beam filling factor.

III. Spaceborne L-Band Doppler-Radiometer: Preliminary Design

In order to verify the validity of the approximations made in the analytical developments, a case study of a spaceborne L-band Doppler-radiometer was studied with spatial resolution $\Delta\rho_{-3\,\mathrm{dB}} = 15$ Km and radiometric sensitivity $\Delta T = 2.1$ K. The following parameters have been used: platform height and speed $H_0 = 800$ km and $v = 7.5$ km/s, baseline $u = v = 242$ wavelengths (50 m baseline), elementary antenna half-power

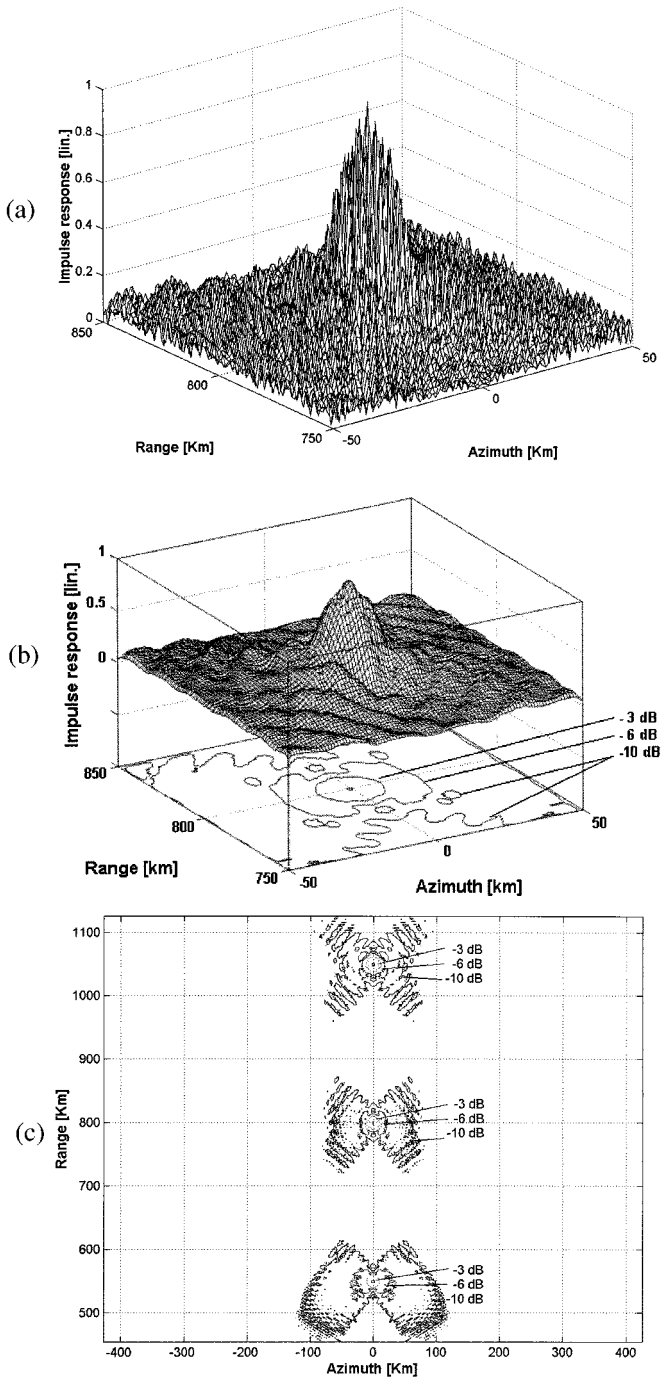

Fig. 4. (a) Impulse response at range $y_0 = 800$ km. A speckle-like effect is apparent. (b) Impulse response at range $y_0 = 800$ km. Idem is as Fig. 4(a) but median-filtered to remove the speckle (contour levels at -3 dB, -6 dB, and -10 dB). (c) Impulse response at range $y_0 = 550$ km, 800 km, and 1050 km (contours at -3 dB, -6 dB, and -10 dB). Pixel size $\Delta x_{-3\,\mathrm{dB}} \cdot \Delta y_{-3\,\mathrm{dB}}$: 7 km $\cdot$ 20 km, 13 km $\cdot$ 13 km, and 25 km $\cdot$ 18 km at $y_0 = 550$ km, 800 km, and 1050 km. Parameters: $H_0 = 800$ km, $\Delta X_{-3\,\mathrm{dB}} = 264$ km, $\Delta Y_{-3\,\mathrm{dB}} = 500$ km, $B = 20$ MHz, $f_0 = 1410$ MHz, $v = 7.5$ km/s, $u = v = 242\lambda$, and $T = 62.4$ s at $y_0 = 800$ km.

[6]Although the emissivity mainly depends on the incidence angle θ_i, it is known that, at least for some surfaces such as the ocean, there is also a small dependence on the azimuth angle ϕ_i.

[7]If 1 bit/two-level correlators are used, the antenna temperature must be approximately constant during the integration time T so as to be able to denormalize μ_{kl} the measured normalized cross-correlation: $V_{kl} = \mu_{kl}\sqrt{(T_A + T_{R1})(T_A + T_{R2})}$.

beamwidth in azimuth $\Delta X_{-3\,\mathrm{dB}} = 264$ km (approximately antenna size $l_x \approx 1.1$ m), swath width[8] $\Delta Y_{-3\,\mathrm{dB}} = 500$ km (approximately antenna size $l_y \approx 0.64$ m), receiver noise bandwidth $B = 20$ MHz, center frequency $f_0 = 1410$ MHz, and system noise temperature 400 K.

With these parameters, at $y_0 = 550$ km, the variation of the incidence angle is $\theta_i = 34.51°-35.36°$ (13), the variation of the azimuth angle is $|\Delta\varphi_i| \leq 14.33°$, and the solid angle subtended by the pixel varies by 4% during the whole measurement (14). The computational load required to focus every pixel is $N = 20$ Giga-samples per receiver (15) and 40 Giga-products, and approximately $\Delta X_{-3\,\mathrm{dB}} \cdot \Delta Y_{-3\,\mathrm{dB}}/\Delta\rho^2_{-3\,\mathrm{dB}} \approx 590$ complex-correlators are required to form the image.

Equation (A1.1) has been evaluated numerically for both $\overline{V}_{12}$ and $\overline{V}_{13}$ with $T = \sqrt{\pi}X/v \approx 63$ s, and $\Delta\tau(t)$ has been computed with the exact expressions (A1.2)–(A1.5) without the approximations made in (A1.6). Fig. 4(a) shows the impulse response at the swath center $y_0 = 800$ km. It suffers from a kind of speckle due to the coherent processing used to focus the pixel. Fig. 4(b) shows the impulse response filtered with a median filter [Fig. 4(a)]. Contour plots are given at -3 dB, -6 dB and -10 dB, and side lobes are just about 4 dB below the maximum.[9] Sidelobes can be reduced by integrating over a longer time interval [no truncation in (A1.13)] and by windowing, which in turn improves radiometric accuracy. Fig. 4(c) shows the contour plot at -3 dB, -6 dB and -10 dB of the impulse response at three different ranges $y_0 = 550$ km, 800 km, and 1050 km. The shape of the pixel is distorted at swath edges, and at $y_0 = 550$ km, the pixel size ($\Delta x_{-3\,\mathrm{dB}} \cdot \Delta y_{-3\,\mathrm{dB}}$) is 7 km $\times$ 20 km, at $y_0 = 800$ km, it is 13 km $\times$ 13 km, and at $y_0 = 1050$ km it is 25 km $\times$ 18 km.

IV. Conclusions

This paper presents the analysis of the 2-D Doppler-radiometer, a concept radiometer that achieves a spatial resolution much higher than the elementary antenna footprint. Spatial resolution in one dimension is achieved by focusing the signals collected by two antennas. An instrumental delay inserted in each element compensates for the differential propagation delay, and the contributions from a given pixel add coherently during the time it is observed by the elementary antennas. 2-D spatial resolution is achieved by forming two crossed baselines and combining both outputs.

Analytical expressions have been derived for the spatial resolution and the radiometric sensitivity. The beam-filling factor being quite small, and high spatial resolution with large antenna footprint degrades the radiometric sensitivity, which is not significantly degraded because of the much longer integration time (antenna footprint divided by the platform speed). Simulation results for a spaceborne L-band radiometer are in good agreement with theoretical formulations when speckle-like artifacts are filtered out. Nonuniform pixel size within the field of view and high sidelobe levels are inherent to other interferometric imaging radiometers [17]. Further work is required to analyze appropriate windows in order to reduce the sidelobes level.

[8]Swath width can be doubled by using to systems pointing to $+\overline{y}$ and $-\overline{y}$ so as not to degrade neither the shape of the shape of the impulse response nor the beam filling factor.

[9]The expression $10\log(\sqrt{\overline{V}_{12}\overline{V}_{13}})$ is used since the output is a power measurement.

Appendix
Impulse Response of a Doppler-Radiometer with Variable Delay Compensation

The correlation between the signals collected by antennas 1–2, corresponding to a pixel located at $(x_0, y_0, 0)$ is given by [1]

$$\begin{aligned}\overline{V}_{12} &= \tfrac{1}{2}\langle b_1(t-\tau_1(t))b_2^*(t-\tau_2(t))\rangle \\ &= kB\,\frac{\Omega_{pix}}{\Omega_{ant}}\,T_{B0}e^{-((y_0-\overline{y})^2/Y^2)}\frac{1}{T}\int_{-T/2}^{T/2} \\ &\quad\cdot e^{-((x_0-vt)^2/X^2)}e^{-\pi B^2\Delta\tau^2(t)}e^{j2\pi f_0\Delta\tau(t)}\,dt \qquad \text{(A1.1)}\end{aligned}$$

where $\tau_1(t) = \hat{r}_1(t)/c$ and $\tau_2(t) = \hat{r}_2(t)/c$ are the estimated delays. See Section II for definition of the above terms.

The delay error is $\Delta\tau(t) = [r_1(t) - \hat{r}_1(t) - r_2(t) + \hat{r}_2(t)]/c$, and

$$r_1(t) = \sqrt{(x_0 - vt - D_1/2)^2 + y_0^2 + H_0^2} \qquad \text{(A1.2)}$$

$$\hat{r}_1(t) = \sqrt{(x_0 - vt - D_1/2 + \Delta x)^2 + (y_0 + \Delta y)^2 + H_0^2} \qquad \text{(A1.3)}$$

$$r_2(t) = \sqrt{(x_0 - vt + D_1/2)^2 + (y_0 - D_2)^2 + H_0^2} \qquad \text{(A1.4)}$$

$$\hat{r}_2(t) = \sqrt{(x_0 - vt + D_1/2 + \Delta x)^2 + (y_0 - D_2 + \Delta y)^2 + H_0^2} \qquad \text{(A1.5)}$$

and $\Delta x = x_1 - x_0$ and $\Delta y = y_1 - y_0$.

The term $r_{1(t)} - \hat{r}_{1(t)} - r_{2(t)} + \hat{r}_{2(t)}$ can be expanded up to second order in t as

$$\begin{aligned}&r_1(t) - \hat{r}_1(t) - r_2(t) + \hat{r}_2(t) \\ &\approx \frac{1}{2}\left(\sqrt{A} + \sqrt{D} - \sqrt{B} - \sqrt{C}\right) \\ &\quad + \left[\frac{D_1 - 2\Delta x}{\sqrt{C}} - \frac{D_1}{\sqrt{D}} + \frac{D_1 + 2\Delta x}{\sqrt{A}} - \frac{D_1}{\sqrt{B}}\right](x_0 - vt) \\ &\quad + \left\{\left[\frac{1}{\sqrt{D}} - \frac{D_1^2}{\sqrt{D^3}}\right] - \left[\frac{1}{\sqrt{C}} - \frac{(D_1 - 2\Delta x)^2}{\sqrt{C^3}}\right]\right. \\ &\qquad \left. - \left[\frac{1}{\sqrt{B}} - \frac{D_1^2}{\sqrt{B^3}}\right] + \left[\frac{1}{\sqrt{A}} - \frac{(D_1 - 2\Delta x)^2}{\sqrt{A^3}}\right]\right\} \\ &\quad \cdot (x_0 - vt)^2 \qquad \text{(A1.6)}\end{aligned}$$

where

$$\begin{aligned}A &= 4D_1\Delta x + 4\Delta x^2 + 4y_0^2 + D_1^2 + 8y_0\Delta y + 4D_2^2 \\ &\quad - 8D_2\Delta y - 8y_0D_2 + 4h_0^2 + 4\Delta y^2 \\ &\approx 4(R_0^2 + 2y_0(\Delta y - D_2)) \qquad \text{(A1.7)} \\ B &= -8y_0D_2 + 4D_2^2 + D_1^2 + 4y_0^2 + 4h_0^2 \\ &\approx 4(R_0^2 - 2y_0D_2) \qquad \text{(A1.8)} \\ C &= -4D_1\Delta x + 4\Delta x^2 + 4y_0^2 + D_1^2 \\ &\quad + 4\Delta y^2 + 4h_0^2 + 8y_0\Delta y \\ &\approx 4(R_0^2 + 2y_0\Delta y) \qquad \text{(A1.9)} \\ D &= 4h_0^2 + 4y_0^2 + D_1^2 \approx 4R_0^2 \qquad \text{(A1.10)}\end{aligned}$$

and

$$R_0 = \sqrt{H_0^2 + y_0^2}.$$

Assuming that Δy, $D_2 \ll R_0$, and y_0, (A1.6) can be simplified to

$$\begin{aligned} r_1(t) - \hat{r}_1(t) - r_2(t) + \hat{r}_2(t) \\ \approx \frac{y_0}{R_0^3}(\Delta x D_2 - \Delta y D_1)(x_0 - vt) \\ + \frac{\Delta x^2}{2R_0^3}(x_0 - vt)^2 \end{aligned} \tag{A1.11}$$

and

$$\Delta\tau(t) \approx \frac{y_0}{R_0^3 f_0}(\Delta x v - \Delta y u)(x_0 - vt) + \frac{\Delta x^2}{2R_0^3 c}(x_0 - vt)^2. \tag{A1.12}$$

Inserting (A1.12) in (A1.1), defining the relative bandwidth $W = B/f_0$, neglecting third and fourth order terms in $(x_0 - vt)$ in the fringe-washing function, we assume that the integrand is negligible outside $[-T/2, T/2]$ so that the limits can be extended to $[-\infty, +\infty]$ as shown in (A1.13) at the bottom of the page.

In the case $W = 0$, (A1.13) is a Gaussian-like function with translation symmetry along the line $\Delta y = v/u\Delta x$ that passes through (x_0, y_0). Along that line, the amplitude is modulated by the term in Δx^4 within the square root of the denominator.

Similarly, for the baseline formed by antennas 1–3, the output of the matched filter is shown in (A1.14) at the bottom of the page, which is another Gaussian-like function with translation symmetry along the line $\Delta y = -v/u\Delta x$ that passes through (x_0, y_0).

Assuming $u = v$ and neglecting the term in Δx within the exponential, the geometric mean of $\overline{V}_{12}$ and $\overline{V}_{13}$ is then shown in (A1.15) at the bottom of the page, where $\Delta x = \Delta\rho\cos\phi$ and

$$\begin{aligned} \overline{V}_{12} &= kB\frac{\Omega_{pix}}{\Omega_{ant}}T_{B0}\exp\left(-\frac{(y_0-\overline{y})^2}{Y^2}\right)\frac{1}{T}\int_{-T/2}^{T/2}\exp\left(-\frac{1}{X^2}\left[1+\pi W^2\left(\frac{y_0X}{R_0^3}\right)^2(\Delta xv-\Delta yu)^2\right](x_0-vt)^2\right) \\ &\quad\cdot\exp\left(j2\pi\left[\frac{y_0}{R_0^3}(\Delta xv-\Delta yu)(x_0-vt)+\frac{\Delta x^2}{2R_0^3\lambda}(x_0-vt)^2\right]\right)dt \\ &= kB\frac{\Omega_{pix}}{\Omega_{ant}}T_{B0}\exp\left(-\frac{(y_0-\overline{y})^2}{Y^2}\right)\frac{\sqrt{\pi}X}{vT}\frac{\exp\left(-\dfrac{\pi^2(y_0/R_0^3)^2(\Delta xv-\Delta yu)^2}{\frac{1}{X^2}\left[1+\left(\frac{\Delta x^2X^2}{R_0^3\lambda}\right)^2+\pi W^2\left(\frac{y_0X}{R_0^3}\right)^2(\Delta xv-\Delta yu)^2\right]}\right)}{\sqrt{1+\left(\frac{\Delta x^2X^2}{R_0^3\lambda}\right)^2+\pi W^2\left(\frac{y_0X}{R_0^3}\right)^2(\Delta xv-\Delta yu)^2}}. \end{aligned} \tag{A1.13}$$

$$\begin{aligned} \overline{V}_{13} &= kB\frac{\Omega_{pix}}{\Omega_{ant}}T_{B0}\exp\left(-\frac{(y_0-\overline{y})^2}{Y^2}\right)\frac{\sqrt{\pi}X}{vT} \\ &\quad\cdot\frac{\exp\left(-\dfrac{\pi^2(y_0/R_0^3)^2(\Delta xv+\Delta yu)^2}{\frac{1}{X^2}\left[1+\pi W^2\left(\frac{y_0X}{R_0^3}\right)^2(\Delta xv+\Delta yu)^2+\left(\frac{\Delta x^2X^2}{R_0^3\lambda}\right)^2\right]}\right)}{\sqrt{1+\pi W^2\left(\frac{y_0X}{R_0^3}\right)^2(\Delta xv+\Delta yu)^2+\left(\frac{\Delta x^2X^2}{R_0^3\lambda}\right)^2}} \end{aligned} \tag{A1.14}$$

$$\begin{aligned} \sqrt{\overline{V}_{12}\overline{V}_{13}} &= kB\frac{\Omega_{pix}}{\Omega_{ant}}T_{B0}\exp\left(-\frac{(y_0-\overline{y})^2}{Y^2}\right)\frac{\sqrt{\pi}X}{vT} \\ &\quad\cdot\frac{\exp\left(-\dfrac{\left(\frac{\Delta\rho}{\varepsilon_\rho}\right)^2+\frac{W^2}{\pi}\left(\frac{\Delta\rho}{\varepsilon_\rho}\right)^4\cos^2(2\phi)}{1+\frac{2}{\pi}W^2\left(\frac{\Delta\rho}{\varepsilon_\rho}\right)^2+\frac{W^4}{\pi^2}\left(\frac{\Delta\rho}{\varepsilon_\rho}\right)^4\cos^2(2\phi)}\right)}{\sqrt{1+2\left(\frac{\Delta x^2X^2}{R_0^3\lambda}\right)^2+\left(\frac{\Delta x^2X^2}{R_0^3\lambda}\right)^4+\frac{2}{\pi}W^2\left(\frac{\Delta\rho}{\varepsilon_\rho}\right)^2\left(1+\left(\frac{\Delta x^2X^2}{R_0^3\lambda}\right)^2\right)+\frac{W^4}{\pi^2}\left(\frac{\Delta\rho}{\varepsilon_\rho}\right)^4\cos^2(2\phi)}} \\ &\approx kB\frac{\Omega_{pix}}{\Omega_{ant}}T_{B0}\exp\left(-\frac{(y_0-\overline{y})^2}{Y^2}\right)\frac{\sqrt{\pi}X}{vT}\exp\left(-\left(\frac{\Delta\rho}{\varepsilon_\rho}\right)^2\right) \end{aligned} \tag{A1.15}$$

$\Delta y = \Delta\rho \sin\phi$, and $\varepsilon_\rho \hat{=} R_0^3/\pi u y_0 X$. The last approximation holds for

$$\frac{2}{\pi} W \frac{\Delta\rho}{\varepsilon_\rho} \ll 1 \quad \text{and} \quad \sqrt{2}\,\frac{\Delta x X}{R_0^{3/2}\lambda^{1/2}} \ll 1.$$

REFERENCES

[1] Y. A. Mel'nik, "Space-time handling of radiothermal signals from radiators that move in the near zone of an interferometer," *Izvestiya Vysshikh Uchebnykh Zavedenii, Radiofiz.*, vol. 15, pp. 1376–1380, Sept. 1972.

[2] ——, "Potential applications of coherent processing of random signals," *Radio Eng. Electron. Phys.*, no. 4, pp. 575–578, 1972.

[3] K. Komiyama, Y. Kato, and T. Iwasak, "Indoor experiment of two-dimensional supersynthesis radiometer," in *Proceedings of the International Geoscience and Remote Sensing Symposium*. Piscataway, NJ: IEEE, 1994, pp. 1329–1331.

[4] K. Komiyama and Y. Kato, "Two-dimensional supersynthesis radiometer for field experiment," in *Proceedings of the International Geoscience and Remote Sensing Symposium*. Piscataway, NJ: IEEE, 1995, pp. 2264–2266.

[5] ——, "Characteristics of the baseline off-nadir angle of supersynthesis radiometer," in *Proceedings of the International Geoscience and Remote Sensing Symposium*. Piscataway, NJ: IEEE, 1996, pp. 875–877.

[6] K. Komiyama, Y. Kato, and K. Furuya, "Interpretation of the brightness temperature retrieved by supersynthesis radiometers," in *Proceedings of the International Geoscience and Remote Sensing Symposium*. Piscataway, NJ: IEEE, 1997, pp. 481–483.

[7] K. Komiyama, "Preliminary experiment of a one-dimensional imaging by microwave supersynthesis radiometer," in *Proceedings of the International Geoscience and Remote Sensing Symposium*. Piscataway, NJ: IEEE, 1998, pp. 1708–1710.

[8] C. R. Edelsohn, "Applications of synthetic aperture radiometry," in *Proceedings of the International Geoscience and Remote Sensing Symposium*. Piscataway, NJ: IEEE, 1994, pp. 1326–1328.

[9] C. Edelsohn, J. Gurley, H. McCord, R. Donnelly, P. Virga, W. Butler, and A. Jain, "RADSDAR (RADiometric SAR) experimental results," in *Proceedings of the International Geoscience and Remote Sensing Symposium*. Piscataway, NJ: IEEE, 1998, pp. 372–374.

[10] A. Camps, F. Torres, J. Bará, I. Corbella, and F. Monzón, "Automatic calibration of channels frequency response in interferometric radiometers," *Electron. Lett.*, vol. 2, no. 35, pp. 115–116, Jan. 21, 1999.

[11] A. R. Thompson, J. M. Moran, and G. W. Swenson, Jr., *Interferometry and Synthesis in Radio Astronomy*: Wiley, 1986, pp. 195–201, 251–258.

[12] W. N. Christiansen and J. A. Högbom, *Radiotelescopes*, 2nd ed. Cambridge, U.K.: Cambridge Univ., 1985, pp. 163–167.

[13] D. M. Alloin and J. M. Mariotti, *Diffraction-Limited Imaging with Very Large Telescopes*. Norwell, MA: Kluwer, 1989, vol. 274, NATO ASI Series, Series C: Mathematical and Physical Sciences, pp. 66–70.

[14] C. S. Ruf, C. T. Swift, A. B. Tanner, and D. M. LeVine, "Interferometric synthetic aperture microwave radiometry for the remote sensing of the earth," *IEEE Trans. Geosci. Remote Sensing*, vol. 26, pp. 597–611, Sept. 1988.

[15] A. Camps, I. Corbella, J. Bará, and F. Torres, "Radiometric sensitivity computation in aperture synthesis interferometric radiometry," *IEEE Trans. Geosci. Remote Sensing*, vol. 35, pp. 680–685, Mar. 1998.

[16] J. B. Hagen and D. T. Farley, "Digital-correlation techniques in radio science," *Radio Sci.*, vol. 8, pp. 775–784, Aug.–Sept. 1973.

[17] SMOS proposal.. [Online]. Available: http://www-sv.cict.fr/cesbio/smos/

Adriano J. Camps (M'00) received the Ing. and Dr.Ing. degrees in telecommunications in 1992 and 1996, both from the Polytechnic University of Catalonia (UPC), Barcelona, Spain.

From 1991 to 1992, he was with the ENS des Télécommunications de Bretagne, France, under an Erasmus Fellowship. In 1993, he joined the Electromagnetics and Photonics Engineering Group, Department of Signal Theory and Communications, UPC, where he is Associate Professor. In 1999, he was on sabbatical at the Microwave Remote Sensing Laboratory, University of Massachusetts, Amherst, as a Visiting Professor. His research interests are focused on passive and active microwave remote sensing, with special emphasis in the microwave imaging radiometer by aperture synthesis (MIRAS), the payload of the SMOS Earth Explorer Opportunity Mission of the European Space Agency. He is currently an Associate Editor for *Radio Science*.

Dr. Camps has received the second Spanish national award of University studies (1993), the "Indra" award of the Spanish Association of Telecommunication Engineers for the best Ph.D. in remote sensing (1997), and as a member of the UPC radiometry group, the "Duran Farell" award for technological research (2000) and the "City of Barcelona" award (2001). He is currently Associate Editor of the IEEE *GRS Newsletter*.

Calvin T. Swift (M'67–SM'69–F'83) was born in Prince William County, VA. He received the S.B. degree from the Massachusetts Institute of Technology, Cambridge, in 1959, the M.S. degree from Virginia Polytechnic Institute, Blacksburg, in 1965, and the Ph.D. degree from the College of William and Mary, Williamsburg, VA, in 1969.

He was a Research Engineer for North American Aviation (now Rockwell International), Downey, CA, from 1959 to 1962, where he worked on a variety of defense and space-related problems. In 1962, he was employed by NASA Langley Research Center, Hampton, VA, where he initially conducted research on plasma-covered antennas. After 1970, he was involved in microwave remote sensing of the Earth, and he assumed leadership responsibility of a microwave radiometer group at Langley. Since 1981, he has been Professor of Electrical and Computer Engineering at the University of Massachusetts, Amherst, and co-founded the Microwave Remote Sensing Laboratory with Prof. R. E. McIntosh. He has published numerous articles and book chapters in the areas of antennas, wave propagation, plasmas, and microwave remote sensing. He was an Associate Editor of the *Journal of Opto-Electronics*

Dr. Swift was elected Vice-Chairman and later Chairman of the United States Commission F (Radio and Nonionized Media) of the International Union of Radio Science (URSI). He served the IEEE Antennas and Propagation Society (AP-S) as Technical Program Chairman of the International AP-S/URSI Symposium held in Williamsburg in 1972, and he was twice elected a member of the AP-S Administrative Committee (AdCom), serving as Meetings Chairman, Secretary-Treasurer, Membership Chairman, and Chairman of Long Range Planning. He was twice elected to the Administrative Committee of the IEEE Geoscience and Remote Sensing Society (GRS-S) and was President of the society in 1985. He has served as a reviewer for many journals and was Guest Editor for the AP-S/JOE (*Journal of Oceanic Engineering*) special joint issue on Radio Oceanography. He is a past Editor of the IEEE TRANSACTIONS ON GEOSCIENCE AND REMOTE SENSING. In 1984, he was awarded a centennial medal from the IEEE. He was also awarded the IEEE Geoscience and Remote Sensing Society Distinguished Achievement Award in 1994.